Two-photon above-threshold ionization of magnesium

A. Reber,[1] F. Martín,[2] H. Bachau,[3] and R. S. Berry[1]
[1]*Department of Chemistry and The James Franck Institute, The University of Chicago, Chicago, Illinois 60637*
[2]*Departamento de Química C-9, Universidad Autónoma de Madrid, 28049 Madrid, Spain*
[3]*Centre Lasers Intenses et Applications (UMR 5107 du CNRS), Université de Bordeaux I, 351 Cours de la Libération, F-33405 Talence, France*
(Received 7 December 2001; published 20 June 2002)

Two-photon above-threshold ionization cross sections and angular distributions have been calculated for Mg in the region between the $3p$ and $4s$ ionization thresholds. We have used the Green's function method in the Feshbach formalism and an L^2 close coupling method, with a basis of L^2 integrable *B*-spline functions. We report the positions, widths, and assignments of a number of $^1S^e$ and $^1D^e$ doubly excited Feshbach states. We have found that correlation is important in the Feshbach states, indicated by significant mixing among configurations, and identified a previously unnoticed "$3d5g$" Feshbach state.

DOI: 10.1103/PhysRevA.65.063413 PACS number(s): 32.80.Rm

I. INTRODUCTION

Although a great deal of experimental and theoretical work has been devoted to understanding the photoionization properties of magnesium [1–8], the problem of above-threshold ionization (ATI) has received less attention [7–10]. It is a process in which an atom absorbs more photons than the minimum number that is required to ionize the atom [11]. The energy may then be transferred either to the ejected electron or into excitation of the core ion. The continuum-continuum transition involved is more difficult to evaluate than bound-continuum transitions, because the wave functions are not localized, and poles may be present in the intermediate-state Green's function.

ATI is a fundamental process in strong-field dynamics, and represents a test for the understanding of correlation effects in continuum states. Our approach permits the study of angular distributions of the ejected electron in ATI and multiphoton ionization processes [10], which is a delicate test of our treatment of correlation. It is an ideal way to study resonant features in the continuum, such as doubly excited Feshbach states and shape resonances.

This study is one of a series in support of recent experiments being performed, which use the photoionization of Mg as an electron source for scattering experiments [12]. In the experiments, ATI processes are difficult to distinguish from scattering processes. The energy of ejected electrons is the same for a scattering process in which an atom deexcites to the ground state, and an ATI process using the photon that pumps the excited state. An in-depth study of various ATI processes in Mg is required to clear up this matter. We also plan to extend this work to include low-energy Mg-e^- scattering. The method we employ also makes it possible to calculate the angular distribution of the ejected electrons in multiphoton ionization [13].

In this work, we evaluate the total and differential cross sections for two-photon ATI in Mg, using an L^2 integrable *B*-spline basis [14]. *B*-splines are a set of piecewise polynomials, which are very effective at simultaneously representing bound and continuum states [15]. We will use the Green's function method in the Feshbach formalism as described by Sánchez and Martín [16]. The intermediate states will be calculated using the L^2 close-coupling approach [17]. We work under the assumption of LS coupling, and use lowest-order perturbation theory (LOPT) in ATI [18]. In this case, we will be dealing with a near-threshold intermediate continuum state. This means the intermediate state will be devoid of resonances, but because of the long wavelength of these low energy states, a basis set that covers large radial distances is required. We are interested in the electronic structure of the relevant Feshbach states; and we describe their positions, widths, and assignments. This method allows for an in-depth study of correlation in the Feshbach states of Mg, in which the importance of correlation has previously been underemphasized.

A great deal of experimental and theoretical work has been performed on the photoionization of Mg. Karapanagioti *et al.* have used both theory and experiment to study population trapping in three-photon ATI in Mg [9,10]. However, they only dealt with a very small energy range in the three-photon ionization spectrum, where only the third photon produces a dipole coupling between two resonances in the continuum. Bonanno *et al.* and Shao *et al.* have also used optical experiments to study the population of doubly-excited states in two-photon ionization of Mg [19,20].

A number of theoretical studies have been performed on the photoionization of Mg, because it may be treated as a relatively simple two-electron structure. Moccia and Spizzo used L^2 methods to evaluate one- and two-photon cross sections; this work was extended by Mengali and Moccia to include core polarization effects [1–5]. Tang *et al.* studied multiphoton ionization of Mg using a *B*-spline configuration interaction approach [6]. Kylstra *et al.* studied resonant processes, including resonantly coupled autoionizing states in Mg [7]. Luc-Koenig *et al.* studied photoionization of Mg, carrying out the only previous study of two-photon ATI, in which they used *R*-Matrix multichannel quantum defect theory [8]. Fang and Ho have studied the doubly excited states below the $3p$ threshold using a *B*-spline configuration interaction method, and Kim and Tayal have studied these autoionizing resonances using *R*-matrix theory [21,22]. In addition to this, Lyras and Bachau have studied the phase

control in 2- and 4-photon ionization in Mg [23]. So, while Mg photoionization has received a great deal of attention, only Luc-Koenig *et al.* have performed an in-depth study of ATI in Mg, and they did not comprehensively study angular distributions.

Atomic units are used throughout, unless otherwise noted. When we designate a state by a single configuration, that is the dominant configuration in our calculation. The correspondence with other identifications is noted.

II. THEORY

The two-photon cross sections are evaluated in the dipole approximation, for linearly polarized light. The cross section for an N photon ionization process is given by

$$\sigma(\mathrm{cm}^{2N}\mathrm{s}^{N-1}) = C^{(N)}\omega^N |M_{g\mu}^{(N)}|^2, \tag{1}$$

where $C^{(2)}$ is a conversion from atomic to traditional units, and is $2.505\,475\times10^{-52}$, ω is the photon energy, and $M^{(2)}$ is the amplitude associated with the two-photon transition between the initial state g and the final channel μ

$$M_{g\mu}^{(2)} = \sum_{\nu} \frac{\langle g|\mathbf{D}\cdot\mathbf{e}|\nu\rangle\langle\nu|\mathbf{D}\cdot\mathbf{e}|\mu\rangle}{E_g+\omega-E_\nu} + \lim_{\eta\to0}\int dE_\nu \frac{\langle g|\mathbf{D}\cdot\mathbf{e}|\nu\rangle\langle\nu|\mathbf{D}\cdot\mathbf{e}|\mu\rangle}{E_g+\omega-E_\nu-i\eta}. \tag{2}$$

Here, ν represents all possible intermediate (bound and continuum) states, g represents the ground state, and $\mathbf{D}\cdot\mathbf{e}$ is the dipole operator. E_g is the energy of the ground state, ω is the photon energy, and E_ν is the energy of the intermediate state. In this work, the velocity gauge of the dipole operator was used throughout. It is clear from Eq. (2) that, if a bound intermediate state lies at the energy $E_g+\omega$, the cross section diverges, which is the well-known failure of LOPT near intermediate resonance states. In ATI, there is always an intermediate state ν with energy $E_g+\omega$; however, no singularity needs to appear in this case. A precise determination of ATI cross sections requires evaluating the pole contribution separately from the principal part value [24]. In this work, we have used a discrete representation of the continuum, which implies that the integral in Eq. (2) turns into a summation. The discretization is then done by varying the box size to ensure that the energies of the true continuum state associated with the pole and its discrete representation match precisely. In practice, the intermediate-state wave functions were calculated using the L^2 integrable close-coupling method, as developed by Cortés and Martín [17]. In the photon energy range considered in this work, there are no intermediate Feshbach or shape resonances, so we found no difficulties with the close-coupling approach.

The final states are treated in the Feshbach formalism [13,25], using the method developed by Sánchez and Martín [16]. In this method, the resonant and nonresonant contributions to the wave functions are treated separately [26]. It permits the calculation of the widths and positions of the doubly excited states in a single calculation. It also makes clear the role of correlation in the spectra by identifying the Feshbach states. The P projection operator selects the nonresonant continuum, and preserves the asymptotic behavior of the stationary continuum wave function, and the Q projection operator selects the doubly excited states and represents bound autoionizing states embedded in the continuum. For each channel μ the exact continuum wave function can be written as

$$|\Psi_{\mu E}^-\rangle = \frac{\langle\phi_s|QHP|P\Psi_{\mu E}^{0-}\rangle}{E-\mathcal{E}_s-\Delta_s(E)-i\Gamma_s(E)/2}|\phi_s\rangle + [1+G_Q^{(s)}(E)QHP]\left\{|P\Psi_{\mu E}^{0-}\rangle + \frac{\langle\phi_s|QHP|P\Psi_{\mu E}^{0-}\rangle}{E-\mathcal{E}_s-\Delta_s(E)-i\Gamma_s(E)/2}G_P^{(s)-}(E)PHQ|\phi_s\rangle\right\}, \tag{3}$$

where $G_Q^{(s)}$ and $G_P^{(s)}$ are the Green's operators associated with their respective space, $|\phi_s\rangle$ is the resonant wave function of energy $\mathcal{E}_s$, $|\Psi_{\mu E}^-\rangle$ is the nonresonant wave function, and E is the energy of the final state; $\mathcal{E}_s$, $\Delta_s(E)$, and $\Gamma_s(E)$ are the exact position, shift, and width of the doubly excited states. The notation explicitly shows that the shift and width are dependent on the energy of the final continuum state. As mentioned above, Eq. (3) is exact and has been used in our evaluation of the two-photon matrix element given in Eq. (2). The resonance parameters presented in the next section have been obtained by choosing $E=\mathcal{E}_s$, which is the usual approximation in the framework of the Feshbach theory [16].

All necessary wave functions were represented in a basis of two-electron states constructed from a B-spline basis. B-splines are an L^2 integrable basis so that this representation results in a discretization of the continuum [15,27]. In this case, for each angular momentum, a basis of 650 B-splines of order 10 was placed in a linear knot sequence with the maximum radius of 250 a.u. The order of the basis refers to the number of nonzero basis functions at each radial point, except at the limit of the box where only the splines vanishing to zero are included. This basis size is significantly larger than previous work with a similar basis [9,10,23]. The basis was large enough that the energy levels and cross sections were essentially invariant with respect to small changes in the basis set. The Mg^{2+} core is represented by an analytic model potential that reproduces the valence-core potential resulting from self-consistent field calculations, plus a phenomenological potential that represents polarization of the core. Details of this model potential can be found in Moccia and Spizzo [28] and Lyras and Bachau [23]. The one-electron states are found by diagonalizing the Mg^+ Hamiltonian using the above B-spline basis set; this diagonalization is performed by imposing orthogonality with the core. The two-electron states appearing in Eq. (3) were then constructed by diagonalizing the Mg Hamiltonian in a basis of configurations built from the one-electron orbitals. The number of two-electron configurations is 100 for each nonresonant continuum channel, and typically 500 for Feshbach resonances. These include orbitals with angular momenta up

through $l=4$. The ground state was calculated using the same one-electron basis as the continuum states.

The angular distributions of the ejected electrons are a rigorous test of the accuracy of our treatment. We use the dipole approximation, and assume that the recoil of the atom is negligible. We also assume that all the photons are linearly polarized, with parallel polarizations. The two-photon differential cross section for Mg is given by

$$\frac{d\sigma_{nl}}{d\Omega}=\beta_0^{nl}P_0(\cos\theta)+\beta_2^{nl}P_2(\cos\theta)+\beta_4^{nl}P_4(\cos\theta). \tag{4}$$

Here, $P_k(\cos\theta)$ represents the kth Legendre polynomial, and the β parameters are given by Eqs. (5)–(7) for the case in which the core ion is left in a $3s$ state [29],

$$\beta_0^{3s}=1, \tag{5}$$

$$\beta_2^{3s}=\frac{10/7|M_{3skd}^{(2)20}|^2+2\sqrt{5}Re|M_{3skd}^{(2)20}||M_{3sks}^{(2)00}|^*}{\sigma_{3s}^{tot}}, \tag{6}$$

$$\beta_4^{3s}=\frac{18/7|M_{3skd}^{(2)20}|^2}{\sigma_{3s}^{tot}}. \tag{7}$$

The case in which the ion is left in the $3p$ state is given by Eqs. (8)–(10) [29],

$$\beta_0^{3p}=1, \tag{8}$$

$$\beta_2^{3p}=\frac{|M_{3pkp}^{(2)20}|^2+8/7|M_{3pkf}^{(2)20}|^2+2Re\{\sqrt{2}|M_{3pkp}^{(2)20}||M_{3pkp}^{(2)00}|^*\}}{\sigma_{3p}^{tot}}+\frac{Re\{\sqrt{3}|M_{3pkp}^{(2)00}||M_{3pkf}^{(2)20}|^*-\sqrt{6}/7|M_{3pkp}^{(2)20}||M_{3pkf}^{(2)20}|^*\}}{\sigma_{3p}^{tot}}, \tag{9}$$

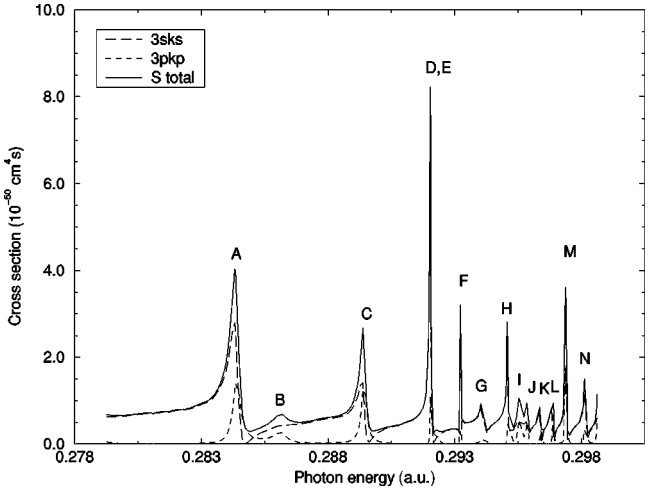

FIG. 1. Two-photon ATI cross sections where $L=0$. The resonances are identified as follows. *A*, $4s7s$; *B*, $3d5d$; *C*, $4s8s$; *D*, $4s9s$; *E*, $4p^2$; *F*, $4s10s$; *G*, $4s11s$; *H*, $4s12s$; *I*, $3d7d$; *J*, $4s14s$; *K*, $4s15s$; *L*, $4s16s$; *M*, $3d8d$.

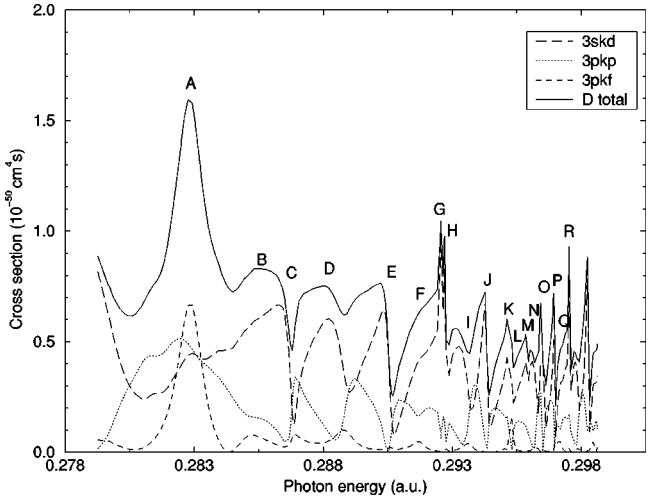

FIG. 2. Two-photon ATI cross sections where $L=2$. The resonances are identified as follows. *A*, $4p^2$; *B*, $3d5d$; *C*, $4s6d$; *D*, $3d7s$; *E*, $4s7d$; *F*, $3d6d$; *G*, $3d4g$; *H*, $4s9d$; *I*, $3d8s$; *J*, $4s10d$; *K*, $3d8d$; *L*, $4s11d$; *M*, $3d5g$; *N*, $4s13d$; *O*, $3d9s$; *P*, $4s14d$; *Q*, $4s15d$; *R*, $3d9d$.

$$\beta_4^{3p}=\frac{6/7|M_{3pkf}^{(2)20}|^2-12\sqrt{6}/7Re\{|M_{3pkp}^{(2)20}||M_{3pkf}^{(2)20}|^*\}}{\sigma_{3p}^{tot}}. \tag{10}$$

The superscripts in the transition amplitudes represent first and in parentheses, the number of photons in the process, and then the angular momentum of the final state and the magnetic quantum number of the final state. It should be noted that in order to calculate the interference terms in Eqs. (6), (9), and (10), the phase shift for the continuum states must be evaluated. This is done by comparing the evaluated wave function with a pure Coulomb wave at a large radial distance [30].

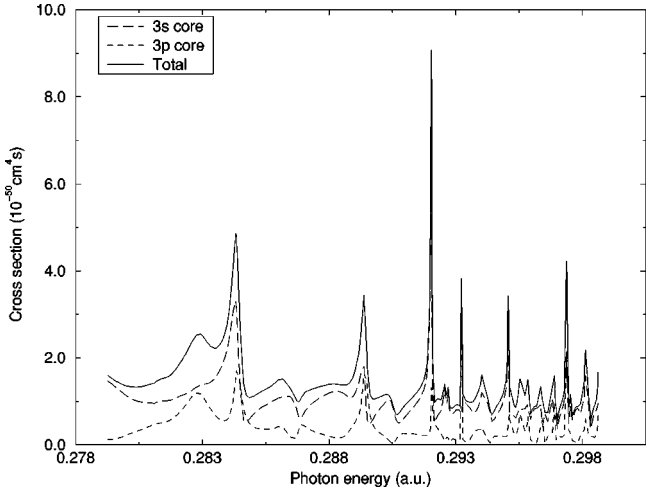

FIG. 3. Two-photon ATI total cross sections for the cases where the ion is left in the $3s$, $3p$ state, and the total two-photon ATI cross section.

TABLE I. A comparison of the position, width, and assignment of doubly excited states in the energy range of interest. Results are from the present work, and Refs. [4] and [8]. (ds) denotes strong mixing between $3dns$ and $4snd$ levels as found by Ref. [4]. Numbers in square brackets indicate powers of ten.

$^1S^e$ Resonances

	Present work			Luc-Koenig *et al.* [8]			Mengali and Moccia [4]		
Label	Conf.	E	Width	Conf.	E	Width	Conf.	E	Width
A	$4s7s$	−0.26319	7.00[−04]	$4s6s$	−0.263087	6.56 [−04]	$4s6s$	−0.26352	6.8[−04]
B	$3d5d$	−0.25964	1.30[−03]	$3d4d$	−0.259224	1.07[−03]	$3d4d$	−0.25919	1.5[−03]
C	$4s8s$	−0.2531	5.16[−04]	$4s7s$	−0.253018	5.70[−04]	$4s7s$	−0.25340	5.5[−04]
D	$4s9s$	−0.24789	3.93[−04]	$4s8s$	−0.247992	1.82[−04]	$3d5d$	−0.24812	1.7[−04]
E	$4p^2$	−0.24755	4.45[−04]	$3d5d$	−0.247409	5.01[−04]	$4s8s$	−0.24711	7.7[−04]
F	$4s10s$	−0.24526	1.14[−05]	$4p^2$	−0.245541	2.05[−05]			
G	$4s11s$	−0.24363	1.87[−04]	$4s9s$	−0.243454	1.28[−04]	$4s9s$	−0.24388	1.1[−04]
H	$4s12s$	−0.24174	8.73[−05]	$4s10s$	−0.241591	7.29[−05]	$3d6d$	−0.24201	7.3[−05]
I	$3d7d$	−0.24088	2.68[−04]	$3d6d$	−0.240752	2.14[−04]			
J	$4s14s$	−0.2402	1.43[−03]	$4s11s$	−0.240005	1.41[−04]			
K	$4s15s$	−0.23915	7.61[−05]	$4s12s$	−0.238993	7.29[−05]			
L	$4s16s$	−0.23819	6.10[−05]	$4s13s$	−0.238214	4.56[−05]			
M	$3d8d$	−0.2372	8.01[−05]	$4s14s$	−0.237613	3.19[−05]			
				$4s15s$	−0.237166	2.28[−05]			
				$3d7d$	−0.236933	1.28[−04]			
				$4s16s$	−0.236711	6.85[−05]			

$^1D^e$ Resonances

	Present work			Luc-Koenig *et al.* [8]			Mengali and Moccia [4]		
Label	Conf.	E	Width	Conf.	E	Width	Conf.	E	Width
A	$4p^2$	−0.26631	2.28[−03]	$4p^2$	−0.267024	2.03[−03]		−0.26639	2.3[−03]
B	$3d5d$	−0.26252	2.82[−03]	$4d^2$	−0.262732	1.82[−03]		−0.26128	2.7[−03]
C	$4s6d$	−0.25836	7.07[−04]	$4s5d$	−0.257934	4.60[−04]	(ds)	−0.25809	5.5[−04]
D	$3d7s$	−0.25425	1.71[−03]	$3d6s$	−0.253893	1.74[−03]	(ds)	−0.25358	1.6[−03]
E	$4s7d$	−0.25082	8.26[−04]	$4s6d$	−0.250512	8.34[−04]		−0.25071	8.7[−03]
F	$3d6d$	−0.24852	1.20[−03]	$3d5d$	−0.24863	9.48[−04]			
G	$3d4g$	−0.24682	1.55[−05]	$3d5g$	−0.246621	2.05[−05]	$3d5g$	−0.24602	1.0[−05]
H	$4s9d$	−0.24643	7.15[−05]	$4s7d$	−0.246192	8.20[−05]	(ds)	−0.24647	1.4[−04]
I	$3d8s$	−0.24463	9.37[−04]	$3d7s$	−0.244434	1.01[−03]		−0.24420	7.3[−04]
J	$4s10d$	−0.24328	4.05[−04]	$4s8d$	−0.24309	5.19[−04]	(ds)	−0.24329	6.4[−04]
K	$3d8d$	−0.24166	5.26[−04]	$3d6d$	−0.241718	4.65[−04]			
L	$4s11d$	−0.24137	2.32[−04]	$4s9d$	−0.241176	2.41[−04]			
M	$3d5g$	−0.24078	3.06[−06]						
N	$4s13d$	−0.24009	9.74[−06]	$4s10d$	−0.239918	9.11[−06]			
O	$3d9s$	−0.23933	3.82[−04]	$3d8s$	−0.239221	4.78[−04]			
P	$4s14d$	−0.2389	2.65[−04]	$4s11d$	−0.238829	4.83[−03]			
Q	$4s15d$	−0.2380	8.97[−05]	$4s12d$	−0.238069	9.57[−05]			
R	$3d9d$	−0.2376	4.35[−04]	$3d7d$	−0.237586	2.00[−04]			
				$4s13d$	−0.237513	1.37[−04]			
				$4s14d$	−0.237034	4.10[−05]			
				$4s15d$	−0.236679	1.37[−05]			

III. RESULTS

We have calculated two-photon ATI cross sections for the energy region between the $3p$ and $4s$ threshold. In this region, the photon energy varies between roughly 0.28 and 0.295 a.u. Here, the $3sks$ $^1S^e$, $3pkp$ $^1S^e$, $3skd$ $^1D^e$, $3pkp$ $^1D^e$, and $3pkf$ $^1D^e$ channels are open. Also, $4skl$, $4pkl$, and $3dkl$ core-excited continuum states may be populated. We used 536 configurations to find a ground-state energy of $-0.830\,959$ a.u. with respect to the Mg^{2+} ion. The Q states were calculated using 381 configurations of $^1S^e$ and 557 configurations for $^1D^e$. The potential was modified to

TABLE II. A list of the significant configurations contributing to each doubly excited state and its amplitude.

S symmetry label	Conf.	Amplitude	D symmetry label	Conf.	Amplitude	S symmetry label	Conf.	Amplitude	D symmetry label	Conf.	Amplitude
A	$4s7s$	0.72	A	$4p^2$	0.62		$4s13s$	−0.41		$3d9s$	−0.32
	$4s6s$	−0.55		$4s5d$	−0.57		$4s10s$	−0.37		$4s10d$	0.27
	$4s5s$	−0.27		$4s6d$	0.26		$3d8d$	−0.2		$3d9s$	−0.24
	$3d5d$	−0.18		$4p4f$	0.22	I	$3d8d$	0.69	J	$4s10d$	0.69
	$3d4d$	0.15		$3d^2$	−0.21		$4s11s$	−0.33		$4s11d$	−0.37
B	$3d5d$	0.81	B	$3d5d$	0.77		$3d7d$	−0.32		$4s8d$	−0.35
	$3d6d$	−0.3		$3d4d$	0.44		$4s13s$	−0.32		$3d8s$	−0.21
	$3d4d$	−0.3		$3d^2$	−0.26		$3d8d$	−0.26	K	$3d8d$	0.61
	$3d^2$	0.26		$3d6d$	−0.2	J	$4s14s$	−0.61		$3d7d$	−0.5
	$4p5p$	−0.2	C	$4s6d$	−0.68		$4s13s$	0.53		$4s11d$	−0.33
	$4s7s$	0.19		$4p^2$	0.33		$4s10s$	−0.26		$3d6d$	−0.26
C	$4s8s$	0.8		$3d6s$	−0.3		$3d8d$	0.24	L	$4s11d$	0.58
	$4s6s$	−0.32		$4s4d$	0.3		$4s12s$	0.22		$4s12d$	−0.5
	$4s9s$	−0.27		$4s7d$	0.25		$4s15s$	0.21		$4s9d$	−0.26
	$4s7s$	−0.26		$3d7s$	0.23	K	$4s15s$	0.7		$3d8d$	0.25
D	$4s9s$	0.59	D	$3d7s$	0.69		$4s13s$	−0.37	M	$3d7g$	0.63
	$3d6d$	−0.5		$3d5s$	−0.40		$4s14s$	−0.34		$3d8g$	−0.59
	$3d7d$	0.37		$4s7d$	−0.33		$4s16s$	−0.32		$3d5g$	−0.37
	$4s10s$	−0.36		$4s6d$	0.3	L	$4s16s$	0.7	N	$4s13d$	−0.59
	$4s6s$	−0.21		$3d5s$	−0.28		$4s14s$	−0.43		$4s12s$	0.49
E	$4p^2$	0.47	E	$4s7d$	0.69		$4s17s$	−0.31		$3d9s$	0.33
	$3d6d$	0.42		$4s8d$	−0.45		$4s11s$	0.24		$4s9d$	−0.25
	$4p5p$	−0.37		$3d6d$	−0.28	M	$3d9d$	0.58	O	$3d9s$	0.51
	$4s7s$	0.34		$3d7s$	0.24		$4s17s$	0.41		$3d10s$	−0.46
	$3d^2$	−0.33		$4s5d$	−0.23		$3d10d$	−0.37		$4s13d$	0.4
	$4d^2$	0.21	F	$3d6d$	0.73		$4s15s$	−0.29		$4s14d$	−0.36
	$3d7d$	−0.21		$3d7d$	−0.46		$3d7d$	0.26	P	$4s14d$	0.64
F	$4s10s$	−0.5		$3d4d$	−0.26					$4s13d$	−0.42
	$3d7d$	−0.43		$4s8d$	−0.23					$4s12d$	−0.36
	$4p^2$	−0.36	G	$3d6g$	0.71					$3d10s$	−0.26
	$3d6d$	0.33		$3d5g$	−0.53				Q	$4s15d$	−0.65
	$4s9s$	0.31		$3d7g$	−0.34					$4s13d$	0.38
	$4s8s$	0.24	H	$4s9d$	0.56					$4s16d$	0.36
G	$4s11s$	0.71		$4s8d$	−0.53					$4s12d$	0.25
	$4s10s$	−0.4		$3d8s$	0.34					$3d9d$	−0.25
	$4s9s$	−0.36		$4s7d$	−0.22				R	$3d9d$	0.69
	$4s12s$	−0.27	I	$3d8s$	0.68					$3d10d$	−0.35
H	$4s12s$	0.71		$4s9d$	−0.4					$3d7d$	−0.33

ensure an accurate calculation of the lowest-energy states of each angular momentum in the Mg^+ ion. Discrepancies between our values and experimental values are likely due to the core potential—the approximation to which the results are likely to be most sensitive. These cross sections for the two-photon ATI process, where $L=0$, are plotted in Fig. 1. The $L=2$ case is plotted in Fig. 2, and the total cross sections for the population of different core states are shown in Fig. 3, $\sigma(3s)=\sigma(3sks\,^1S^e)+\sigma(3skd\,^1D^e)$, and $\sigma(3p)=\sigma(3pkp\,^1S^e)+\sigma(3pkp\,^1D^e)+\sigma(3pkf\,^1D^e)$. These plots show reasonable general agreement with the R-matrix multichannel quantum-defect theory results of Ref. [8]. However, significantly different profiles can be observed in the $L=2$ case for peak C and beyond. The dominant feature of these spectra is a series of Feshbach resonances that increase in density as the $4s$ threshold is approached. A list of the position, widths, and tentative assignments of the resonances is listed in Table I. A comparison between the present results, and previous calculations from Luc-Koenig *et al.* [8] and Moccia and Mengali [4] is also shown. Table II lists the significant configurations and amplitudes of each Feshbach state.

The $^1S^e$ symmetry results are dominated by the $3sks\ ^1S^e$ channel, and a series of Feshbach resonances. These results show reasonable agreement with previous results, although

there is some disagreement on the precise assignment and position of the resonances. We generally assigned the resonances to a configuration with a slightly higher n quantum number. We also found a great deal of mixing among states. This shows that the electron correlation is important in these Feshbach states, especially the radial correlation. A significant example of this is in the "$4s9s$," "$4p^2$," and "$4s10s$" states. The "$4s9s$" state was assigned to be "$4s8s$" by Luc-Koenig, and "$3d5d$" by Mengali and Moccia. The analysis of the compononents showed this state to have a significant contribution from the $3d6d$ configuration. We found the "$4p^2$" state also to have a significant $3d6d$ component, and in fact, the $3dnd$ components dominate. In this state, there is even a non-negligible $4f^2$ component. The "$4s10s$" state also showed significant $4p^2$, $3d7d$, and $3d6d$ components. An additional difference is that we found the "$4s9s$" state to shift to a lower energy level than the "$4p^2$" state due to coupling with the continuum. This causes "$4s9s$" and "$4p^2$" to overlap one another. Because previous results show a slightly larger separation between these two states, this may prove to be an interesting focus for an experimental study. Overlapping resonances are not separate entities, but are a superposition of two Feshbach states and the continuum at nearly the same energy. Our description of this phenomenon is accurate because, in contrast with standard applications of the Fano or Feshbach theories, Eq. (3) is exact and, therefore, we are not assuming that the resonances are well separated in energy. However, the Feshbach-like form of Eq. (3) allows us to infer values of parameters with the same meaning as for isolated resonances. Despite the differences in assignment, the energies and widths of the resonances show good agreement with previous theoretical work.

Our results for the ${}^1D^e$ symmetry cross sections also show reasonable agreement with previous results. The broad $4p^2$ resonance structure is the most noticeable feature, and it shows strong coupling to the $3pkf$ channel. It is also interesting to note that a number of $4snd$ and $3dns$ Feshbach states produce transparencies in the $3skd$ continuum. There is some additional disagreement of the assignment of the resonances. This is again due to the importance of correlation, or it may be due to differences in the one-electron spectra between the methods. We do find an additional "$3d5g$" resonance not found by Luc-Koenig *et al*. This demonstrates a nice feature of the Feshbach method; the Feshbach resonances are determined directly. This could also be due to our larger box size, so that our description of diffuse wave functions may be somewhat more accurate. The difference in box size may also explain some of the disagreement with the R-matrix calculation for the resonance profiles.

The total cross section for each ion state is plotted in Fig. 3. The $3skl$ continua have consistently higher cross sections than the $3pkl$ continua.

The angular distributions of the ejected electrons are plotted in Figs. 4 and 5. In Fig. 4, the case where the ion is left in a $3s$ state is shown, and in Fig. 5, the case where the ion is left in a $3p$ state is shown. A major change in the angular distributions is expected when encountering a resonance, because the correlation changes drastically when approaching a resonance. In the case where the core is left in the $3s$ state,

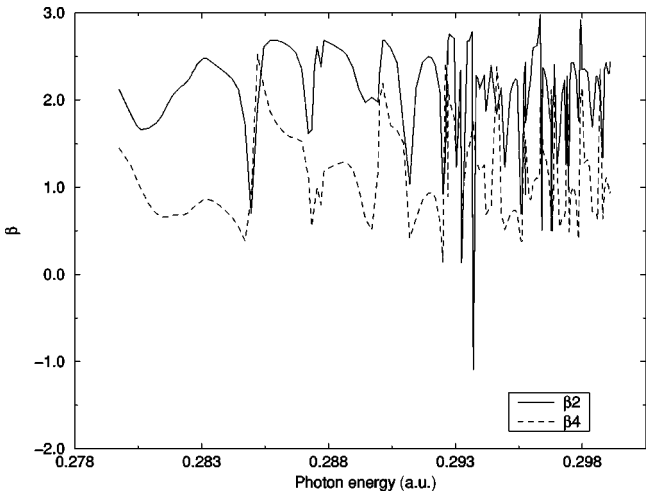

FIG. 4. Two-photon ATI angular distributions for the case where the ion is left in the $3s$ state.

we see that the angular distributions are anisotropic. Luc-Koenig *et al.* have only reported the values of these asymmetry parameters in the vicinity of the $4p^2$ resonance. Our results for this resonance are somewhat similar to theirs, although we appear to use a different convention in defining the β parameters. Nonetheless, the results appear to be consistent. The origin of this discrepancy is not clear to us, although it may be due to differences between using jj coupling and LS coupling. As the density of the Feshbach states increase, predicting the angular distributions becomes extremely difficult. In the $3p$ case, we do not see much agreement between our results and the two cases discussed by Luc-Koenig *et al*. This again may be due to the differences between using jj coupling and LS coupling, but also to a deficient description of electron correlation because, as is well known, the angular distribution of the ejected electrons is strongly dependent on this property.

IV. CONCLUSIONS

We have studied the two-photon above-threshold ionization of Mg between the $3p$ and $4s$ threshold using an L^2

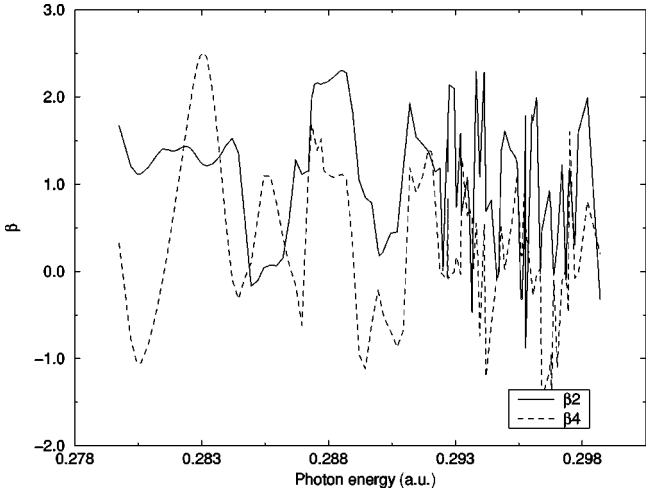

FIG. 5. Two-photon ATI angular distributions for the case where the ion is left in the $3p$ state.

integrable *B*-spline basis in the Feshbach formalism. This case requires that the intermediate state lies very near the $3p$ threshold. Because we are dealing with low-energy free states, the basis must cover an unusually large radius for convergence. We show that this method has been highly successful in describing multiphoton ionization in two-electron atoms. The cross sections found in this study show reasonable agreement with previous results. We also provide a comprehensive study of the angular distributions of the ejected electrons. We found that the correlation plays a more important role in the Feshbach states in this region than previous results had indicated. We found a great deal of radial mixing in all of the Feshbach states, and even a great deal of angular mixing in some of the $^1S^e$ states surrounding the "$4p^2$" Feshbach state. We also found an additional "$3d5g$" resonance, which suggests that our method may more accurately describe highly diffuse Feshbach states than *R*-matrix methods. Finally, our results suggest that this region, especially in the neighborhood of the "$4s9s$" $^1S^e$ and "$4p^2$" $^1S^e$ Feshbach states, should prove to be an interesting subject for an optical experiment.

ACKNOWLEDGMENTS

The authors would like to thank Tahllee Baynard and Scott Darveau for useful discussions and experimental motivation. This work was supported by the National Science Foundation, GAANN (A.R.), the Ministerio de Ciencia y Tecnología, Project No. BFM2000-0033, and the Comisión de Intercambio Cultural, Educativo y Científico entre España y los Estados Unidos de América.

[1] R. Moccia and P. Spizzo, J. Phys. B **21**, 1121 (1988).
[2] R. Moccia and P. Spizzo, J. Phys. B **21**, 1133 (1988).
[3] R. Moccia and P. Spizzo, J. Phys. B **21**, 1145 (1988).
[4] S. Mengali and R. Moccia, J. Phys. B **29**, 1597 (1996).
[5] S. Mengali and R. Moccia, J. Phys. B **29**, 1613 (1996).
[6] X. Tang, T.N. Chang, P. Lambropoulos, S. Fournier, and L.F. DiMauro, Phys. Rev. A **41**, 5265 (1990).
[7] N.J. Kylstra, H.W. van der Hart, P.G. Burke, and C.J. Joachain, J. Phys. B **31**, 3089 (1998).
[8] E. Luc-Koenig, A. Lyras, J.M. Lecomte, and M. Aymar, J. Phys. B **30**, 5213 (1997).
[9] N.E. Karapanagioti, O. Faucher, Y.L. Shao, D. Charalambidis, H. Bachau, and E. Cormier, Phys. Rev. Lett. **74**, 2431 (1995).
[10] N.E. Karapanagioti, D. Charalambidis, C.J.G.J. Uiterwaal, C. Fotakis, H. Bachau, I. Sánchez, and E. Cormier, Phys. Rev. A **53**, 2587 (1996).
[11] P. Agostini, F. Fabre, G. Mainfray, G. Petite, and N.K. Rahman, Phys. Rev. Lett. **42**, 1127 (1979).
[12] S. Darveau and R.S. Berry, *Resonance Ionization Spectroscopy* (AIP, Woodbury, NY, 1998).
[13] I. Sánchez, H. Bachau, and F. Martín, J. Phys. B **30**, 2417 (1997).
[14] C. De Boor, *A Practical Guide to Splines* (Springer, New York, 1978).
[15] H. Bachau, E. Cormier, P. Decleva, J. Hansen, and F. Martín, Rep. Prog. Phys. **64**, 1601 (2001).
[16] I. Sánchez and F. Martín, Phys. Rev. A **44**, 7318 (1991).
[17] M. Cortés and F. Martín, J. Phys. B **27**, 5741 (1994).
[18] E. Cormier, H. Bachau, and J. Zhang, J. Phys. B **26**, 4449 (1993).
[19] R.E. Bonanno, C.W. Clark, and T.B. Lucatorto, Phys. Rev. A **34**, 2082 (1986).
[20] Y.L. Shao, C. Fotakis, and D. Charalambidis, Phys. Rev. A **48**, 3636 (1993).
[21] T.K. Fang and Y.K. Ho, J. Phys. B **32**, 3863 (1999).
[22] D.S. Kim and S. Tayal, J. Phys. B **33**, 3235 (2000).
[23] A. Lyras and H. Bachau, Phys. Rev. A **60**, 4781 (1999).
[24] H. Bachau, P. Lambropoulos, and X. Tang, Phys. Rev. A **42**, 5801 (1990).
[25] I. Sánchez, F. Martín, and H. Bachau, J. Phys. B **28**, 2863 (1995).
[26] H. Feshbach, Ann. Phys. (N.Y.) **19**, 287 (1962).
[27] O.K. Rice, J. Chem. Phys. **1**, 375 (1933).
[28] R. Moccia and P. Spizzo, Phys. Rev. A **39**, 3855 (1989).
[29] C. Liu, N. Du, and A. Starace, Phys. Rev. A **43**, 5891 (1991).
[30] F. Martín and A. Salin, Chem. Phys. Lett. **157**, 146 (1989).